Doubly Selective Vehicle-to-Vehicle Channel Measurements and Modeling at 5.9 GHz

Guillermo Acosta-Marum, Mary Ann Ingram

School of Electrical and Computer Engineering, Georgia Institute of Technology
Atlanta, GA 30332-0250, USA

gacosta@gatech.edu
mai@ece.gatech.edu

***Abstract*—A method to develop a commercial channel emulator model for a doubly selective vehicle-to-vehicle wireless channel is presented. This channel can apply to vehicular ad hoc networks (VANETs) and intelligent transportation applications. The model was developed from measurements taken at 5.9 GHz in an expressway environment when the vehicles are traveling in the same direction. The probe waveform is a combination of a direct sequence spread spectrum (DSSS) waveform with an orthogonal frequency division multiplexing (OFDM) waveform with a chirp signal for pulse compression.**

Key words: propagation modeling; 802.11p; Doppler spectra; channel identification; doubly-selective.

1. Introduction

In this paper, we consider the identification of channel models for the vehicle-to-vehicle (VTV) channel, such that the models are suitable for certain commercial RF channel emulators and computer simulators. Such channels are found in vehicular ad hoc networks (VANETs), and are of growing interest as the new IEEE 802.11p standard [1] nears completion. The modulation for 802.11p is orthogonal frequency division multiplexing (OFDM), at 5.9 GHz, with a bandwidth of 10 MHz. Therefore, the channels for 802.11p are doubly selective, which means they are both time- and frequency-selective. Applications for 802.11p include alerts for approaching emergency vehicles, collision avoidance, and forced braking for road hazards (possibly triggered by the braking occurring in vehicles in front of the driver on the expressway). Other applications for VANETs include battleground communications [2] and mobile sensor networks [3], [4].

The type of model we consider is the tapped delay line, where each tap process is described as having Rician or Rayleigh fading, and by a Doppler power density spectrum (PSD). Certain RF channel emulators, such as the SPIRENT 5500 [5], and certain communication system simulators, such as MATLAB Simulink, describe doubly selective channels in terms of "paths," where the Doppler PSD of each path is described as having one of a small collection of shapes, such as "Classic 6 dB," "Rounded," or "Flat" [5]. Other path parameters include the shape's width, center frequency, excess delay, and area (*i.e.* path power). One can craft a "composite" tap PSD by assigning several paths with different shapes to have the same excess delay. However, an RF channel emulator has only a finite number of paths; older models have only 12 paths and newer models, such as the 5500, have 24 paths. If multiple-antenna nodes are being modelled, then these paths must be divided among the antennas, further limiting the number of paths per channel model. Therefore, in defining channel models for this type of channel emulator, only one to three paths per tap should be used. This paper investigates one way to make these definitions, and that for 802.11p, for some taps, at least two shapes must be used in order to capture the features of the channel that are critical to link performance.

Previous work related to VTV measurement and modelling include theoretical 2-D [6] and 3-D [7] VTV models, flat-fading VTV measurements for the highway [8], and doubly selective models for the roadside-to-vehicle channel [9]. In [9], the authors report Doppler spectrum shapes, but they do not describe how those shapes were determined. Power delay profiles (PDPs) and tap fading statistics were reported in [10]. Preliminary models based on measurements taken in 2003 at 2.4 GHz of the expressway with same-direction travel and a high middle wall were reported in [11], [12] and [13]. [12] and [13] report attempts to capture the wide range of link BER variation with a collection of tapped delay lines.

2. Description of the Measurements and Initial Processing

The data used in this paper were measured at 5.9 GHz using a probe waveform that alternated between two types of sounding waveforms: a 511-long maximum length sequence direct-sequence spread spectrum (DSSS) waveform and an OFDM with 512-point FFT waveform using a chirp signal for pulse compression [14]. The purpose of this is so that the DSSS waveform can be used to synchronize the OFDM waveform. As we will explain

later, the OFDM waveform provides twice the delay resolution of the DSSS waveform. For the results in this paper, the DSSS waveform was also used to estimate the PDP and the OFDM waveform was used to estimate the Doppler spectra of the taps.

The transmit and receive antennas were 8 dBi monopoles, magnetically mounted to the roofs of two vans. The transmit power was +43 dBm. The receiver performed a frequency downconversion to a 1 GHz first IF. The first IF signal was then downconverted to a second IF of 10 MHz by an Advance Radio Model ADV3000T, which had a 3 dB RF bandwidth of 40 MHz. The output of the Advance Radio was then sampled with 12 bits and at a rate of 80 MHz. These samples were then input to a Pentek Digital Radio, which produced complex baseband samples at a rate of 20 Msamples/sec. Rubidium clocks were used to synchronize the receiver to the transmitter.

Each data recording was 9.6 seconds long. These records, or "takes" were further divided for convenience into 0.6 second-long "segments" for processing. The received waveform for each segment was split into its DSSS and OFDM parts.

For the available 20 MHz bandwidth, the time resolution of the DSSS waveform is 100 ns. The spectrum of this signal is double-sided; therefore, we require two samples per symbol in the recorder. The DSSS part was correlated to the chip sequence, and the output of the correlator was arranged into an impulse response matrix such that each row was a channel impulse response taken at a certain time (i.e. certain position of the cars) and each column represented a particular delay in the impulse response. The length of the DSSS sequence provides a dynamic range of 54 dB.

We also inserted a 320-length null signal between the two sounding waveforms. Counting the OFDM ¼ guard-band, the total length of the combined waveform is as long as 2,302 50ns chips. This length produces a repetition rate of 8.688 KHz, yielding a maximum unambiguous Doppler frequency of ±4.344 KHz. Because of the complex bandwidth of the OFDM waveform, we only need one sample per symbol in the recorder. Theoretically, this should provide a time resolution of 50ns considering the 20 MHz bandwidth of the OFDM signal. However, we found that the dynamic range of the PDPs derived from the OFDM signal had high sensitivity to imperfect calibration of the recording system. Therefore, we used the PDP of the DSSS signal. In spite of the aliasing of the DSSS waveform in the receiver (because of the 10MHz IF), the DSSS waveform still provides a better PDP estimate than the OFDM waveform. We used the more bandlimited OFDM to get the Doppler spectrum because of the available 4X oversampling, which translated into a cleaner Doppler spectrum.

The expressway same-direction site was used for the results in this paper. This site data contained 21 total takes from several different expressway locations in the metro Atlanta, Georgia area, all with approximately 400 m separation between the vehicles, with and average vehicle speed of 100.3 km/hr (62.3 mph).

3. Modeling Approach

The magnitude squared of each element of the DSSS-based impulse response matrix was averaged down the columns to provide a power delay profile (PDP) for each segment. A threshold of approximately 30 dB relative to the peak of the PDP was applied to eliminate noise effects in the PDP. Samples below the threshold were set to zero. Then the PDPs were averaged across segments and takes to create the "overall PDP." Again, a 30 dB threshold is applied to the overall PDP. The bins with power greater than this threshold are called the significant taps of the overall PDP, and they become the taps of the final model for the site.

Next, the power spectral density (PSD) for each significant tap in each segment is found. One way to proceed from here is to average the PSDs for a given tap across the segments and takes, yielding an average PSD for that tap for the site. However, the Doppler frequency of the line-of-sight (LOS) component causes a problem with this approach [13]. The Doppler frequency of the LOS component varies from segment to segment as the relative velocity of the vehicles changes. Because of the changing Doppler of the LOS, the averaged spectrum ends up having a broad peak which would not correspond to a Rician characteristic if that spectrum were used as a basis for channel simulation. In other words, a significant K factor is indicated in a tap PSD by a spectral line. If a PSD without a narrow line is used as a basis for a filter in the filtered white noise approach to tap process simulation [15], then the measured K factor for that simulated tap would be insignificant.

In [13], we dealt with this problem for the expressway same-direction channel by aligning the spectra (i.e. translating them in frequency) before averaging, such that the peaks of the aligned spectra were all at zero Doppler. Then we averaged those spectra and ignored the somewhat less broad peak in our subjective shape-fitting process. Since the same translation should not necessarily apply to all spectral components, we decided to take a different and more objective approach in this paper.

In this paper, we estimate the K factor of each bin in each segment using the moment method [16], and we use this as a basis for removing the spectral peak. The K factor is the ratio of the power of the "deterministic" or dominant spectral component over the power of the random or diffuse reflection component. We note that the method of moments approach measures the relative power of any phase or frequency modulated component; it is not necessary that the component have zero Hz Doppler. Using the K factor, we calculate the fraction of power that is attributed to the deterministic component. By incrementally

lowering a horizontal line, starting at the spectral peak, we can identify the level such that the PSD area above this line equals the deterministic power and the area below equals the random power. We then store the separated parts of the spectrum and store the frequency of the peak for each segment. Finally, by averaging the random parts across segments and takes, we can arrive at an average random spectral part for the site. We can also produce an average of the deterministic parts, which shows the range of variation of the spectral line frequency and also shows the influence of the segments with a particularly strong LOS. Alternatively, we can produce a histogram of spectral peak locations.

Our approach to identifying the shape of the random part of the spectrum is based on the limitations of the RF channel emulators and by the type of link (OFDM) that is being evaluated. Usually, the identified channel model is intended to be an inherent property of the channel, and applicable to any type of air interface with a similar RF frequency and bandwidth. Therefore, propagation modellers are usually interested in the geometrical properties of the channel, such as the distinct parameters of each path of propagation, such as its power, delay and angle of arrival. However, our objective is only to characterize the tap spectra, within the limited delay resolution of the target system and the limited degrees of freedom of the RF channel emulator. The delay resolution (100ns) of our measurements is large and corresponds to 30 m of excess path distance, which will include many actual paths of propagation with different Doppler shifts. Furthermore, for OFDM, if the excess delay is within the guard interval and if the channel frequency response nulls are not too deep, then the primary channel impairment to the link will be the inter-carrier interference (ICI) caused by the Doppler spreads of the tap processes [17]. This impairment can be quantified based on the Doppler spectrum. Therefore, in our modelling approach, we will attempt to optimally fit to the measured tap spectrum.

With such limited degrees of freedom in the fitting process, some parts of the spectrum will not be matched well. Therefore, the question arises, should certain parts of the spectrum be considered as more important than others? For this, we will use a weighting function that would match the ICI of the measured and modelled channels, if every tap had the same spectrum (i.e. assuming a separable channel).

Assuming also that the Doppler spectra are symmetrical, Cai and Giannakis [17] give the following expression for the average interference power that a signal on subcarrier *k* makes on subcarrier *m*:

$$\psi_q = \pi^{-2} E_s \int_0^1 \varphi_n(f) \sin^2(\pi f_d T_s f) \left[\frac{1}{(f_d T_s f + q)^2} + \frac{1}{(f_d T_s f - q)^2} \right] df \quad (1)$$

where $q = m - k$ and $\varphi_n(f)$, $0 \le f \le 1$, is a normalized version of the spectrum, such that $2\int_0^1 \varphi_n(f) df = 1$, and $\varphi_n(f) = f_d \varphi(f_d f)$, where $\varphi(f)$ is the original Doppler spectrum, except normalized to unit area.

The main observation is that for 802.11p, and vehicle speeds of about 143 km/hr, $f_d T_s \approx 0.01$, which means that (1) simplifies to

$$\psi_q \approx \frac{2E_s (f_d T_s)^2}{q^2} \int_0^1 \varphi_n(f) f^2 df \quad (2)$$

This expression tells us that the higher frequencies in the Doppler spectrum contribute more to the ICI, as indicated by the weighting by the square of the frequency. It also tells us that the effect of the distance between subcarriers (q) is decoupled from the Doppler spectrum effects. Finally, we note that the square root of twice the integral is the Doppler spread.

Suppose that $\varphi_n'(f)$ and ψ_q' are the proposed RF channel emulator spectrum and its corresponding ICI, respectively. We can consider the difference between the ICI values produced by the two spectra:

$$\left|\psi_q - \psi_q'\right| \approx \frac{2E_s (f_d T_s)^2}{q^2} \left| \int_0^1 [\varphi_n(f) - \varphi_n'(f)] f^2 df \right| \quad (3)$$

The choices of shape, center frequency, and width of the RF channel emulator spectrum impact only the integral. By the triangle inequality, we have:

$$\left|\psi_q - \psi_q'\right| \le \frac{2E_s (f_d T_s)^2}{q^2} \int_0^1 |\varphi_n(f) - \varphi_n'(f)| f^2 df, \quad (4)$$

which suggests the cost function:

$$\left(\int_0^1 |\varphi_n(f) - \varphi_n'(f)| f^2 df \right)^{-1}. \quad (5)$$

For each tap, we employed the genetic algorithm [18] to optimize (5) over the channel emulator spectrum parameters for one or two paths, under the constraint that the areas of $\varphi_n(f)$ and $\varphi_n'(f)$ are held constant.

Prior to optimization, we set to zero all measured spectrum values for |f| > 1200 Hz, to avoid fitting to noise. We defined the domain of the optimization to be |f| < 1500 Hz to force the spectrum shapes to be within the +/- 1500 Hz window.

4. Results and Discussion

Figure 1 shows the overall PDP for the site. There are 8 significant bins or taps. Figure 2 shows one snapshot of the Doppler spectrum for Tap 1, illustrating the level method of Rician component removal. There is still a broad peak remaining, which may be there because of shifting of the Doppler frequency of the LOS over the 0.6 s segment. Figure 3 shows the histogram of Doppler frequencies of the LOS for the 334 segments. The Doppler varies roughly from -100 Hz to +100 Hz. Figure 4 shows the averaged deterministic part of the Tap 1 spectrum. The level and hole methods coincide except for the four small peaks on the left. The frequencies of these small peaks are less than -200 Hz, indicating that the level method clipped more than just

one peak in at most four out of 334 segments. The different shapes of the histogram vs. the averaged spectrum in Figure 3 and Figure 4, indicate that the LOS Doppler was apparently more powerful when it was farther away from zero Hz.

Figure 5 and Figure 6 are the histogram and averaged deterministic spectrum for Tap 4. We observe Rician components with Doppler frequencies as large as about 1200 Hz in magnitude. This frequency corresponds to twice the vehicle speed, and results from reflections from stationary objects, such as bridges, that are nearly directly in front of or directly behind the two traveling vehicles. The two curves in Figure 6 are very close, indicating little multi-peak clipping by the level method.

Figure 7 and Figure 8 show histograms of the K factors for Taps 1 and 4. We observe an especially wide variation in K factor for Tap 1, ranging from zero to about 95. For Tap 4, the variation is more limited, but clearly indicates that for many segments, the later taps in the model have significant K factors. If the K factors for the segments are simply averaged, as they were in [13], the results are 12.0, 2.1, 1.7, 1.3, 0.78, 0.55, 0.22, 0.15, for Taps 1 through 8, respectively. On the other hand, if the ratio of averaged areas is used, the values are much lower, yielding for example 2.52 for Tap 1; using this method the K factors for many later taps are so small that a Rayleigh fading assumption is appropriate.

Figure 9 shows the result of the genetic algorithm fit of two path spectra to the average of the random spectrum parts produced by the level method. These are both "rounded" spectra. The result for the single path spectrum ("one shape") fit is very similar to just the narrow rounded shape of Figure 9, except it is almost imperceptively (at the scale of this figure) taller and wider. The difference in dB of the ICI power between measured and shape-fitted spectra indicates how important it is to have two shapes when optimizing under a constraint of same PSD area: for Tap 1, the difference is 11.52 dB for a one shape fit and 6.23 dB for a two-shape fit.

To complete the model specification, a spectral line needs to be added to the first tap spectrum, with a power according to the K factor 2.52 and with a frequency selected based on the distributions in Figure 3 and Figure 4, for example the mean of Figure 1 could be used. This spectral line should not be added as a pure frequency shift, which is an option for a path with the SPIRENT 5500, because through laboratory testing, we determined that this will not produce the desired Rician characteristic. Rather it should be added by making one of the paths, say the one with the wide spectral shape, be a Rician path. The K factor for that path will be much larger than 2.52, but should be so that the K factor for the whole tap is 2.52. Also one- or two-shape spectra should be determined for the other seven taps.

5. Conclusions

An approach to channel identification for the purpose of RF channel emulation and Simulink simulation has been described for the vehicle-to-vehicle channel in the expressway, same-direction travel scenario. Because of limited degrees of freedom in spectrum fitting, a weighting function was used to ensure that the ICI for OFDM that is produced by the model tap is as near as possible to that of the measured channel, given a constraint on tap power. With this weighting function, it is clear that at least two shapes per tap are necessary to model the first tap of the model.

The histograms of K factors given in the paper show a wide range of variation, even in later taps. However, since for most of the segments, the K factors are low, then the K factors based on average powers are low, and can be approximated as zero for all taps but the first.

Acknowledgment

The authors gratefully acknowledge the support for this work provided by ARINC, Inc., Contract No. DTFH6199-C-00018.

References

[1] ASTM E 2213-03, "Standard Specification for Telecommunications and Information Exchange between Roadside and Vehicle Systems— 5.9 GHz Band Dedicated Short Range Communications (DSRC) Medium Access Control (MAC) and Physical Layer (PHY) Specifications," ASTM International, www.astm.org.

[2] Ramanathan, R.; Redi, J.; Santivanez, C.; Wiggins, D.; Polit, S., "Ad hoc networking with directional antennas: a complete system solution," IEEE Journal on Selected Areas in Communications, Volume 23, Issue 3, pp. 496 – 506, March 2005.

[3] Heo Nojeong and P. K. Varshney, "Energy-efficient deployment of intelligent mobile sensor networks," IEEE Transactions on Systems, Man and Cybernetics, Vol. 35, No. 1, pp. 78–92, January 2005.

[4] H. Gharavi and K. Ban, "Multihop sensor network design for wide-band communications," IEEE Proceedings, Vol. 91, No. 8, pp. 1221–1234, August 2003.

[5] Spirent Communications SR5500 Wireless Channel Emulator Operations Manual. www.spirentcom.com

[6] C. S. Patel, G. L. Stüber, and T. G. Pratt, "Simulation of Rayleigh faded mobile-to-mobile communication channels," in Proc. of IEEE Vehicular Technology Conf., vol.1, pp. 163-167, October 2003.

[7] F. Vatalaro and A. Forcella, "Doppler spectrum in mobile-to-mobile communications in the presence of three-dimensional multipath scattering," IEEE Trans. on Vehic. Tech., vol. 46, no. 1, pp. 213-219, 1997.

[8] J. Maurer, T. Fügenm and W. Wiesbeck, "Narrow-band measurement and analysis of the inter-vehicle transmission channel at 5.2 GHz," in Proc. of IEEE Vehicular Technology Conf., vol. 3, pp. 1274-1278, 2002.

[9] X. Zhao, J. Kivinen, P. Vainikainen, and K. Skog, "Characterization of Doppler spectra for mobile communications at 5.3 GHz," IEEE Trans. Vehicular Technology, vol. 52, no. 1, pp. 14-23, 2003.
[10] Matolak, D.W.; Indranil Sen; Wenhui Xiong; Yaskoff, N.T., "5 GHZ Wireless Channel Characterization for Vehicle to Vehicle Communications," IEEE Military Communications Conference, 2005, Page(s):1 – 7, 17-20 Oct. 2005.
[11] G. Acosta, K. Tokuda, and M. A. Ingram, "Measured joint Doppler-delay power profiles for vehicle-to-vehicle communications at 2.4 GHz," in Proc. of IEEE Global Telecom. Conf., vol. 6, pp. 3813-3817, 2004.
[12] Guillermo Acosta and Mary Ann Ingram, "Model development for the wideband vehicle-to-vehicle 2.4 GHz channel," Proc. IEEE Wireless Communications & Networking Conference (WCNC 2006), Las Vegas, NV, 3-6 April 2006.
[13] G. Acosta-Marum and M.A. Ingram, "A BER-Based Partitioned Model for a 2.4 GHz Vehicle-to-Vehicle Expressway Channel," in International Journal on Wireless Personal Communication, July 2006.
[14] J.D. Parsons, D.A. Demery, and A.M.D. Turkmani, "Sounding techniques for wideband mobile radio channels: a review," *IEE Proceedings*, vol. 138, no. 5, pp. 437-446, 1991.
[15] M. C. Jeruchim, P. Balaban, and K. S. Shanmugan, Simulation of Communication Systems: Modeling, Methodology, and Techniques, Second Edition, Kluwer Academic Press, Boston 2000.
[16] L. J. Greenstein, D. G. Michelson, and V. Erceg, "Moment-method estimation of the Ricean *K*-factor," in *IEEE Communications Letters*, vol. 3, No. 6, pp. 175-176, June 1999.
[17] X. Cai and G.B. Giannakis, "Bounding performance and suppressing intercarrier interference in wireless mobile OFDM," IEEE Trans. Comm. Vol. 51, No. 12, December 2003.
[18] http://ideas.repec.org/c/cod/matlab/ga.html

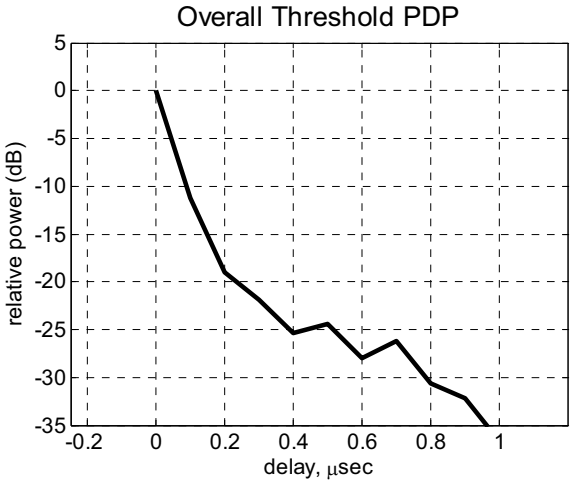

Figure 1: The overall power delay profile (PDP) for the expressway, same-direction travel scenario.

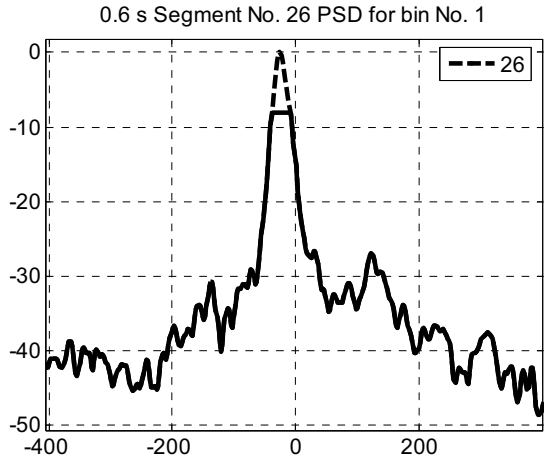

Figure 2: An example spectrum estimate for a 0.6 second segment. The flat part indicates the level corresponding to the K factor measured for this segment.

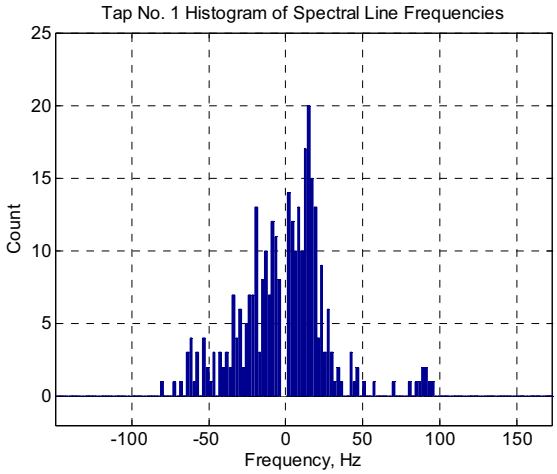

Figure 3: Histogram of Rician component frequencies for Tap. No. 1

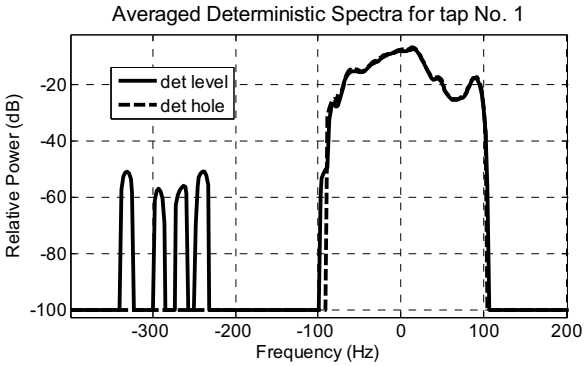

Figure 4: Average of the parts of the spectra that were removed by the level and hole methods for Tap. No. 1

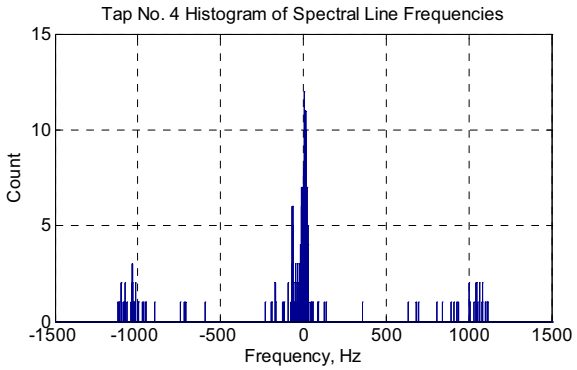

Figure 5: Histogram of Rician component frequencies for Tap No. 4

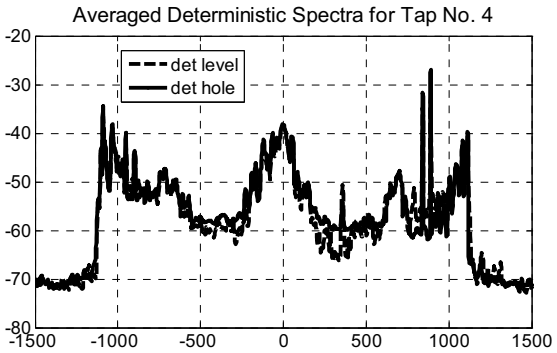

Figure 6: Average of the parts of the spectra that were removed by the level and hole methods for Tap. No. 1

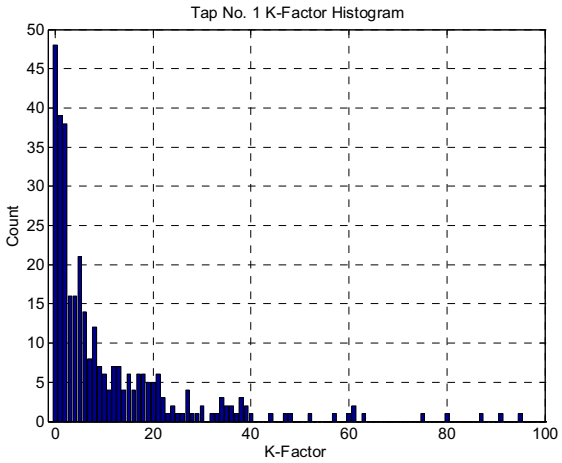

Figure 7: Histogram of K factor values for Tap. 1.

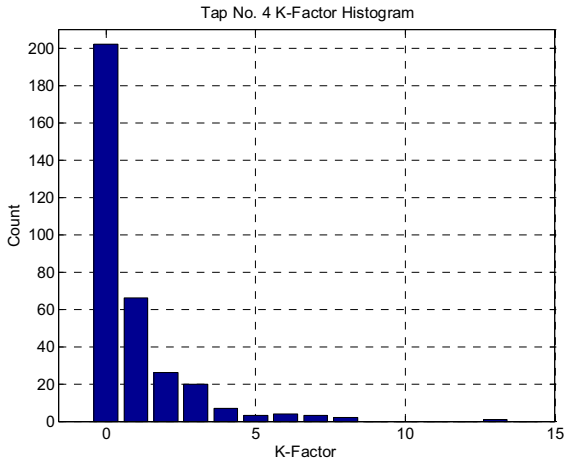

Figure 8: Histogram of K factor values for Tap 4.

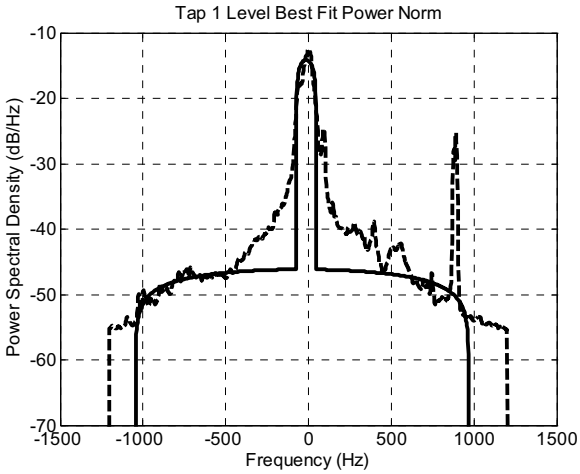

Figure 9: Two-shape fit to the random part spectrum of Tap. No. 1.